

## Production of hidden-charm strange pentaquarks $P_{cs}$ from the $K^- p \rightarrow J/\psi \Lambda$ reaction

Samson Clymton,<sup>1,\*</sup> Hee-Jin Kim,<sup>1,†</sup> and Hyun-Chul Kim<sup>1,2,‡</sup>

<sup>1</sup>*Department of Physics, Inha University, Incheon 22212, Republic of Korea*

<sup>2</sup>*School of Physics, Korea Institute for Advanced Study (KIAS), Seoul 02455, Republic of Korea*

 (Received 17 February 2021; revised 30 April 2021; accepted 3 July 2021; published 30 July 2021)

We investigate the production of the hidden-charm pentaquark  $P_{cs}^0(4459)$  with strangeness in the  $K^- p \rightarrow J/\psi \Lambda$  reaction, employing two different theoretical frameworks, i.e., the effective Lagrangian method and the Regge approach. Having determined all relevant coupling constants, we are able to compute the total and differential cross sections for the  $K^- p \rightarrow J/\psi \Lambda$  reaction. We examine the contributions of  $P_{cs}$  with different sets of spin-parity quantum number assigned. The present results may give a guide for possible future experiments.

DOI: [10.1103/PhysRevD.104.014023](https://doi.org/10.1103/PhysRevD.104.014023)

### I. INTRODUCTION

Very recently, the LHCb Collaboration has announced the finding of a new hidden-charm pentaquark state with strangeness in the analysis of  $\Xi_b^- \rightarrow J/\psi \Lambda K^-$  decays [1]. This hidden-charm pentaquark baryon with strangeness is christened as  $P_{cs}^0(4459)$ . The mass and width of  $P_{cs}$  is determined to be respectively  $4458.8 \pm 2.9_{-1.1}^{+4.7}$  MeV and  $17.3_{-5.7}^{+8.0}$  MeV. While the quark content of  $P_{cs}^0(4459)$  can be given as  $udsc\bar{c}$ , its spin-parity quantum number is not known yet because of lack of the data. This finding broadens our understanding of how the quarks form multi-quark hadrons in addition to the heavy pentaquark baryons  $P_c$  [2–4] and many charmoniumlike tetraquark mesons [5,6] (see recent experimental and theoretical reviews [7–11]). The structure of  $P_c$  and  $P_{cs}$  has been theoretically studied in various works [12–35]. The internal structure of the hidden-charm pentaquark states is still under debate. Since the mass of  $P_{cs}^0(4459)$  is about 19 MeV below the  $\bar{D}^* \Xi_c^0$  threshold, it is arguably considered to be a hadronic molecular state [18,21–26]. On the other hand, the hidden-charm pentaquark states are interpreted as compact pentaquarks consisting of two diquarks and an antiquark bound states [12–14,17,36], hadrocharmonium states [37–39], coupled-channel unitary approach with the local hidden gauge formalism [27,28], five-quark

states [29–31], meson-baryon molecules with coupled channels [32], meson-baryon molecules coupled to the five-quark states [33,34], and as hadronic molecule states in a quasipotential Bethe-Salpeter equation approach [35]. Theoretically, the spin-parity quantum number of the  $P_{cs}^0(4459)$  is proposed to be  $1/2^-(3/2^-)$ . Reference [25] argues that  $J^P = 3/2^-$  is preferable over  $J^P = 1/2^-$  based on the hadronic molecular picture of  $P_{cs}^0(4459)$ , though it should be determined by experiments.

In principle, the hidden-charm pentaquark states can be produced by meson beams such as the pion and kaon. Since several experimental programs to measure charmed hadrons have been planned at the Japan Proton Accelerator Research Complex (J-PARC) [40–44], it is also of great importance to investigate the production mechanism of the hidden-charm pentaquark states. In Ref. [45], the production of the  $P_c^0(4380)$  and  $P_c^0(4450)$  was studied in the  $\pi^- p \rightarrow J/\psi n$  reaction, based on the effective Lagrangian approach. This approach provides a simple but clear understanding of how the  $P_c$ 's can be created at the level of the Born approximation. The transition amplitude includes the  $P_c$ 's as the resonance baryons in the  $s$  channel explicitly together with  $\pi$  and  $\rho$  exchanges in the  $t$  channel and the  $P_c$ 's exchange in the  $u$  channel. They found that the contributions of the  $P_c^0(4380)$  and  $P_c^0(4450)$  bring about the clear peak structures in order of  $1 \mu\text{b}$  at the energies corresponding to the masses of  $P_c$ 's. On the other hand, Ref. [46] examined the  $\pi^- p \rightarrow J/\psi n$  reaction, using the Regge approach. The  $t$  channel for the hidden charm reaction is distinguished from that for the open charm reaction, since the hidden charm processes are suppressed by the Okubo-Zweig-Iizuka (OZI) rule. This indicates that it is difficult to determine the coupling constant for  $P_c$  by

\*sclymton@inha.edu

†heejin.kim@inha.edu

‡hchkim@inha.ac.kr

Published by the American Physical Society under the terms of the [Creative Commons Attribution 4.0 International license](https://creativecommons.org/licenses/by/4.0/). Further distribution of this work must maintain attribution to the author(s) and the published article's title, journal citation, and DOI. Funded by SCOAP<sup>3</sup>.

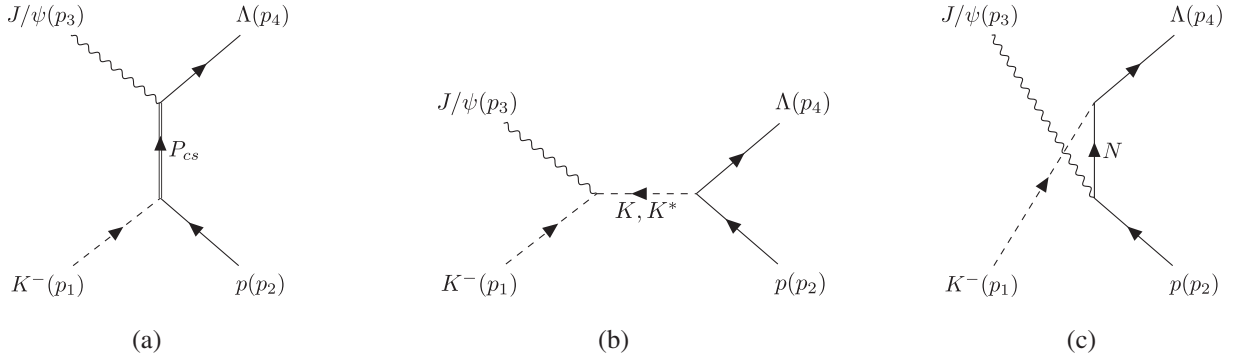


FIG. 1. The tree-level Feynman diagrams for the  $K^- + p \rightarrow J/\psi + \Lambda$  reaction. In the left panel the  $s$ -channel is drawn, whereas in the center and right panels, the  $t$ -channel and  $u$ -channel diagrams are depicted.  $p_i$  stand for the four-momenta of hadrons involved in the reaction.

using some model calculations. Thus, one needs to make a reasonable assumption for the branching ratios of  $P_{cs}$ . A similar situation is expected also for the  $K^- p \rightarrow J/\psi \Lambda$  reaction.

In the present work, we investigate the production of  $P_{cs}^0(4459)$  in the  $K^- p \rightarrow J/\psi \Lambda$  reaction, based on two different theoretical models, i.e., the effective Lagrangian method and Regge approach. In particular, since the energy of the initial kaon should be enough to create the charmonium  $J/\psi$  and  $\Lambda$ , it is worthwhile to consider also the Regge approach. In Refs. [42,43], both the effective Lagrangian method and Regge approach were used for the study of the open-charm process  $\pi^- p \rightarrow D^{*-} \Lambda_c^+$ . It turns out that the Regge approach describes the experimental data very well over the whole energy region. However, while the Regge approach describes the general behavior of the cross sections at very high energies, it has certain difficulties to describe experimental data quantitatively. One effective way of improving this Regge approach is that one can replace the Feynman propagators in the transition amplitudes derived based on the effective Lagrangian by the Reggeized propagator. This method is often called the hybridized Regge approach. Actually, the Regge approach was used for the description of the  $\pi^- p \rightarrow J/\psi n$  reaction [47] in which the total cross section for the reaction was estimated to be around 1 pb at the momentum  $p = 50$  GeV/c. Moreover, the hybridized Regge approach was developed and successfully applied to photoproduction of mesons [48]. In the present work, we take the same strategy such that we will employ both the effective Lagrangian and Regge approaches and compare the results each other, since these two approaches are complementary each other. Since the spin-parity quantum number of  $P_{cs}^0(4459)$  is experimentally unknown, we will consider six different cases, i.e.,  $J^P = 1/2^\pm$ ,  $J^P = 3/2^\pm$ , and  $J^P = 5/2^\pm$ , emphasizing the cases of  $J^P = 1/2^-$  and  $3/2^-$ . Then, we scrutinize the differences among the contributions of  $P_{cs}$  to the  $K^- p \rightarrow J/\psi \Lambda$  with the different spin-parity quantum number assigned. The present work

will provide helpful guidance on possible future experiments at the J-PARC and on determining the spin-parity quantum number of  $P_{cs}$ .

We sketch the present work as follows: In Sec. II, we explain the general formalism for the effective Lagrangian and Regge approaches. Since the coupling constants at the vertices including  $P_{cs}$  are not known, we first estimate them by imposing reasonable assumptions on the branching ratios of the  $P_{cs}$  decays. In Sec. III, we present the results for the total and differential cross sections, emphasizing the differences arising from different spin-parity quantum numbers. In the final section, we summarize the present work and will draw conclusions.

## II. GENERAL FORMALISM

We first start with the effective Lagrangian approach and then will continue to formulate the transition amplitude for the  $K^- p \rightarrow J/\psi \Lambda$  reaction in the Regge approach.

### A. Effective Lagrangian method

In the effective Lagrangian approach for the  $K^- p \rightarrow J/\psi \Lambda$  reaction, we can consider three different Feynman diagrams that are drawn in Fig. 1. In the  $s$  channel, we can only include  $P_{cs}^0(4459)$  with the experimental data on its mass and decay width taken into account [1]. Though we can include other hyperons with strangeness  $S = -1$ , we will neglect them, because we do not have any information on the coupling constant for the vertices such as  $Y \Lambda J/\psi$  and furthermore their contributions will be negligible, since they are far from on-mass-shell. The  $t$  channel contains  $K$  and  $K^*$  exchange. In the  $u$  channel, we can introduce the nucleon. Note that it is not possible to include  $P_{cs}$  in the  $u$  channel, which is very different from the case of the  $\pi^- p \rightarrow J/\psi n$  reaction. Since the spin-parity quantum number of  $P_{cs}^0(4459)$  is unknown, we assume six different cases:  $J^P = 1/2^\pm, 3/2^\pm, 5/2^\pm$ . Taking into account these different quantum numbers, we can express the effective Lagrangians for  $P_{cs}$  as follows [45,46,49–51]

$$\begin{aligned}
 \mathcal{L}_{P_{\Lambda J/\psi}^{1/2\pm}} &= -g_{P_{\Lambda J/\psi}} \bar{P} \Gamma_{\mu}^{\mp} \Lambda \psi^{\mu} + \frac{f_{P_{\Lambda J/\psi}}}{2m_{\Lambda}} \bar{P} \sigma_{\mu\nu} \Gamma^{\pm} \Lambda \psi^{\mu\nu} + \text{H.c.}, \\
 \mathcal{L}_{P_{\Lambda J/\psi}^{3/2\pm}} &= -\frac{g_{P_{\Lambda J/\psi}}}{2m_{\Lambda}} \bar{P}_{\mu} \Gamma_{\nu}^{\pm} \Lambda \psi^{\mu\nu} - \frac{f_{P_{\Lambda J/\psi}}}{4m_{\Lambda}^2} \bar{P}_{\mu} \Gamma^{\mp} \partial_{\nu} \Lambda \psi^{\mu\nu} \\
 &\quad - \frac{h_{P_{\Lambda J/\psi}}}{4m_{\Lambda}^2} \bar{P}_{\mu} \Gamma^{\mp} \Lambda \partial_{\nu} \psi^{\mu\nu} + \text{H.c.}, \\
 \mathcal{L}_{P_{\Lambda J/\psi}^{5/2\pm}} &= -\frac{g_{P_{\Lambda J/\psi}}}{2m_{\Lambda}^2} \bar{P}_{\mu\alpha} \Gamma_{\nu}^{\mp} \Lambda \partial^{\alpha} \psi^{\mu\nu} - \frac{f_{P_{\Lambda J/\psi}}}{4m_{\Lambda}^3} \bar{P}_{\mu\alpha} \Gamma^{\pm} \partial_{\nu} \Lambda \partial^{\alpha} \psi^{\mu\nu} \\
 &\quad - \frac{h_{P_{\Lambda J/\psi}}}{4m_{\Lambda}^3} \bar{P}_{\mu\alpha} \Gamma^{\pm} \Lambda \partial^{\alpha} \partial_{\nu} \psi^{\mu\nu} + \text{H.c.}, \quad (1)
 \end{aligned}$$

where  $P$ ,  $\Lambda$ ,  $\psi^{\mu}$  denote the fields corresponding respectively to  $P_{cs}^0(4459)$ ,  $\Lambda^0$ , and  $J/\psi$ .  $\psi_{\mu\nu}$  is defined as  $\partial_{\mu}\psi_{\nu} - \partial_{\nu}\psi_{\mu}$ .  $m_{\Lambda}$  stands for the mass of the  $\Lambda$  hyperon.  $\Gamma_{\mu}$  and  $\Gamma$  are given respectively by

$$\Gamma_{\mu}^{\pm} = \begin{pmatrix} \gamma_{\mu} \gamma_5 \\ \gamma_{\mu} \end{pmatrix} \quad \text{and} \quad \Gamma^{\pm} = \begin{pmatrix} 1 \\ i\gamma_5 \end{pmatrix}, \quad (2)$$

with different parities considered. Since we consider the production of  $P_{cs}$  in the vicinity of the  $J/\psi\Lambda$  threshold, we will take into account the first terms in each effective Lagrangians. We will consider only the terms with  $g_{P_{\Lambda J/\psi}}$  in the effective Lagrangian, assuming that those with  $f_{P_{\Lambda J/\psi}}$  and  $h_{P_{\Lambda J/\psi}}$  are rather small near the threshold.

The effective Lagrangians for the  $NP_{cs}K$  vertex are written as

$$\begin{aligned}
 \mathcal{L}_{P_{NK}^{1/2\pm}} &= -g_{P_{NK}} \bar{P} \Gamma^{\mp} N K + \text{H.c.}, \\
 \mathcal{L}_{P_{NK}^{3/2\pm}} &= -\frac{g_{P_{NK}}}{M_{P_{cs}} m_N} \epsilon^{\mu\nu\alpha\beta} \partial_{\mu} \bar{P}_{\nu} \Gamma_{\alpha}^{\pm} N \partial_{\beta} K + \text{H.c.}, \\
 \mathcal{L}_{P_{NK}^{5/2\pm}} &= -\frac{g_{P_{NK}}}{M_{P_{cs}} m_N^2} \epsilon^{\mu\nu\alpha\beta} \partial_{\mu} \bar{P}_{\nu\rho} \Gamma_{\alpha}^{\mp} N \partial^{\rho} \partial_{\beta} K + \text{H.c.}, \quad (3)
 \end{aligned}$$

where  $M_{P_{cs}}$  and  $m_N$  represent the masses of  $P_{cs}$  and the nucleon respectively.

Since there is no information on the coupling constants for the  $P_{cs}J/\psi\Lambda$  and  $P_{cs}KN$  vertices experimentally, it is very difficult to determine them. As will be discussed soon, one possible way is to resort to some guess work based on theoretical works [46,52,53] and recent experimental data on  $\pi N$  and  $\bar{K}N$  scattering [54–56]. Note that we have used the  $\pi N$  and  $\bar{K}N$  scattering data to extrapolate the  $P_{cs}J/\psi\Lambda$  and  $P_{cs}KN$  coupling constants. This is an assumption justified by the fact that the energy of the  $P_{cs}$  production is rather high such that the effects of the explicit SU(3) symmetry breaking are also suppressed, considering the fact that the ratio between the strange current quark mass  $m_s$  and the kinetic energy of the  $\Lambda$  baryon, is rather small. The coupling constants for  $P_{cs}$  are extracted by using the partial-wave decay width given by

$$\Gamma(P_{cs} \rightarrow MB) = \frac{|\mathbf{k}|}{8\pi M_{P_{cs}}^2} \frac{1}{2J+1} \sum_{\lambda_1=-J}^J \sum_{\lambda_2, \lambda_3} |A(P_{cs} \rightarrow MB)|^2, \quad (4)$$

where  $M$  and  $B$  denote the produced meson and baryon in the final state, respectively.  $|\mathbf{k}|$  is the momentum of the meson in the final state and  $J$  represents the total angular momentum of the final state. The  $\lambda_i$  are the spin projections of the particles involved. The decay amplitudes  $A(P_{cs} \rightarrow MB)$  for  $P_{cs} \rightarrow J/\psi\Lambda$  are obtained from the effective Lagrangian with spin-parity quantum numbers for  $P_{cs}$  given

$$\begin{aligned}
 A_{P_{\Lambda J/\psi}^{1/2\pm}} &= -g_{P_{\Lambda J/\psi}} \bar{u}_P \Gamma_{\mu}^{\mp} \epsilon^{\mu} u_{\Lambda}, \\
 A_{P_{\Lambda J/\psi}^{3/2\pm}} &= i \frac{g_{P_{\Lambda J/\psi}}}{2m_{\Lambda}} \bar{u}_{P\mu} \Gamma_{\nu}^{\pm} (q_{\psi}^{\mu} \epsilon^{\nu} - q_{\psi}^{\nu} \epsilon^{\mu}) u_{\Lambda}, \\
 A_{P_{\Lambda J/\psi}^{5/2\pm}} &= \frac{g_{P_{\Lambda J/\psi}}}{2m_{\Lambda}^2} \bar{u}_{P\mu\alpha} \Gamma_{\nu}^{\mp} (q_{\psi}^{\mu} \epsilon^{\nu} - q_{\psi}^{\nu} \epsilon^{\mu}) q_{\psi}^{\alpha} u_{\Lambda}, \quad (5)
 \end{aligned}$$

whereas those for  $P_{cs} \rightarrow KN$  are expressed as

$$\begin{aligned}
 A_{P_{NK}^{1/2\pm}} &= -g_{P_{NK}} \bar{u}_P \Gamma^{\mp} u_N, \\
 A_{P_{NK}^{3/2\pm}} &= -\frac{g_{P_{NK}}}{M_{P_{cs}} m_N} \epsilon_{\mu\nu\alpha\beta} \bar{u}_P^{\mu} q_P^{\nu} \Gamma_{\pm}^{\alpha} q_K^{\beta} u_N, \\
 A_{P_{NK}^{5/2\pm}} &= i \frac{g_{P_{NK}}}{M_{P_{cs}} m_N^2} \epsilon_{\mu\nu\alpha\beta} \bar{u}_P^{\nu\rho} q_P^{\mu} \Gamma_{\mp}^{\alpha} q_K^{\beta} q_{K\rho} u_N. \quad (6)
 \end{aligned}$$

$\epsilon_{\mu}$  in Eq. (5) stands for the polarization vector of  $J/\psi$ .  $q_i^{\mu}$  ( $i = P, K, \psi$ ) denote respectively the momenta of  $P_{cs}$ ,  $K$  and  $J/\psi$  in the center of mass (CM) frame. Note that  $P_{cs}$  is at rest before it decays. The Rarita-Schwinger spinor for  $P_{cs}$  with higher spins ( $s \geq 3/2$ ) is given by the following recursive equation [57]

$$\begin{aligned}
 u_{\mu_1 \dots \mu_{n-1}\mu}^{n+1/2}(p, s) &\equiv \sum_{r, m} (n+1/2, s | 1, r; n-1/2, m) \\
 &\quad \times u_{\mu_1 \dots \mu_{n-1}}^{n-1/2}(p, m) \epsilon_{\mu}^r(p), \quad (7)
 \end{aligned}$$

where  $s$ ,  $m$  and  $r$  designate the projections of spin- $(n+1/2)$ , spin- $(n-1/2)$ , and the polarization of a massive spin-1 particle respectively.

To determine the coupling constants for the  $P_{cs}J/\psi\Lambda$  and  $P_{cs}KN$  vertices, one should know the experimental data on their branching ratios. Unfortunately, however, they are not known at all. Even in the case of the  $P_c$  its branching ratios are unknown experimentally. This means that we have to make reasonable assumptions of the branching ratios of  $P_{cs} \rightarrow J/\psi\Lambda$  and  $P_{cs} \rightarrow KN$ . A previous investigation on photoproduction of the hidden-charm pentaquark  $P_c(4450)$  [52] proposed that if the branching ratio of  $P_c(4450) \rightarrow J/\psi p$  is 1% or less, then one can explain the threshold enhancement of the  $J/\psi$

TABLE I. Numerical results for the coupling constants  $g_{P_{cs}J/\psi\Lambda}$  and  $g_{P_{cs}KN}$ . The branching ratios of  $P_{cs} \rightarrow J/\psi\Lambda$  and  $P_{cs} \rightarrow pK$  decays are assumed to be 1% and 0.01%, respectively. Note that we choose the positive values for the coupling constants.

$g_{P_{cs}MB}(J^P)$	$1/2^+$	$1/2^-$	$3/2^+$	$3/2^-$	$5/2^+$	$5/2^-$
$P_{cs}J/\psi\Lambda$	$1.26 \times 10^{-1}$	$4.41 \times 10^{-2}$	$1.48 \times 10^{-1}$	$5.46 \times 10^{-2}$	$1.33 \times 10^{-1}$	$3.83 \times 10^{-1}$
$P_{cs}Kp$	$5.82 \times 10^{-3}$	$3.77 \times 10^{-3}$	$2.06 \times 10^{-3}$	$3.18 \times 10^{-3}$	$1.84 \times 10^{-3}$	$1.19 \times 10^{-3}$

production due to  $P_c$  and the modification of the  $J/\psi$  mass in nuclear medium. However, this is still a very crude estimate for the branching ratio of  $P_c \rightarrow J/\psi p$ . Note that even the  $\pi^- p \rightarrow J/\psi n$  reaction was not much studied experimentally and only the upper limit of its total cross section is known [54,55]. Nevertheless, in Refs. [46,53], the upper limit of the total cross section for the  $\pi^- p \rightarrow J/\psi n$  reaction was cautiously investigated with  $P_c$  resonances taken into account, in which the constraint on the branching ratio of  $P_c$  was discussed, especially in the region near the threshold. The branching ratio of  $P_c \rightarrow J/\psi n$  decay was estimated to be about a few percent whereas  $P_c \rightarrow \pi^- p$  decay was given to be of order  $10^{-4}$ , since it is the OZI-suppressed process. These estimates are in agreement with recent findings from the GlueX Collaboration [58].

When it comes to that for  $P_{cs}$  decays, the situation is even worse than the  $P_c$  case. Since there is no experimental information on the decay of  $P_{cs}$  at all, it is very difficult to determine the coupling constant for the  $P_{cs}J/\psi\Lambda$  and  $P_{cs}KN$  vertex. Nevertheless, it is worthwhile to estimate the branching ratio of the  $P_{cs} \rightarrow J/\psi\Lambda$ . Since the threshold energy of the  $P_{cs}$  production is rather high, the effects of the explicit SU(3) symmetry breaking are also suppressed, considering the fact that the ratio between the strange current quark mass  $m_s$  and the kinetic energy of  $\Lambda$ ,  $T_K(\Lambda)$ , is rather small ( $m_s/T_K(\Lambda) \ll 1$ ). Actually, this assumption is a reasonable one, since the magnitude of the total cross section of  $K^- p$  scattering is similar to  $\pi^- p$  scattering [56]. Based on this assumption, we are able to estimate the upper limit of the total cross section for the  $K^- p \rightarrow J/\psi\Lambda$  reaction near threshold to be around 1 nb. This implies that the branching ratios of the  $P_{cs} \rightarrow J/\psi\Lambda$  and  $K^- p$  decays are about 1% and 0.01% respectively. If the branching ratio of  $P_{cs} \rightarrow J/\psi\Lambda$  were larger than 10%, then one would have found the evidence for the existence of  $P_{cs}$  already from the old data for  $K^- p$  scattering, which we will discuss later. Moreover, note that this 1% branching ratio of the  $P_{cs} \rightarrow J/\psi\Lambda$  decay is in line with recent investigations on the structure of  $P_{cs}$  with the molecular picture taken into account [26,59].

Using this estimate of the branching ratio, we can obtain the coupling constant for the  $P_{cs}KN$  vertex. The results for the coupling constants for  $P_{cs}$  are listed in Table I. Note that we take the positive values for the coupling constants.

Once the values of the coupling constants are given, it is straightforward to express the transition amplitudes in the  $s$  channel

$$\mathcal{M}_{1/2^\pm} = ig_{P_{cs}J/\psi}g_{P_{cs}KN}\bar{u}(p_4, \lambda_4)\Gamma_{\mp}^{\mu}\epsilon_{\mu}^*(p_3, \lambda_3)\frac{\not{q} + M_{P_{cs}}}{s - M_{P_{cs}}^2} \times \Gamma_{\mp}u(p_2, \lambda_2), \quad (8)$$

$$\mathcal{M}_{3/2^\pm} = -\frac{g_{P_{cs}J/\psi}g_{P_{cs}KN}}{2M_{P_{cs}}m_Nm_{\Lambda}}\bar{u}(p_4, \lambda_4)\Gamma_{\nu}^{\pm}(p_3^{\mu}\epsilon^{*\nu}(p_3, \lambda_3) - \epsilon^{*\mu}(p_3, \lambda_3)p_3^{\nu})\frac{\Delta_{\mu\sigma}}{s - M_{P_{cs}}^2}\epsilon^{\rho\sigma\alpha\beta}q_{\rho}\Gamma_{\alpha}^{\pm}p_{1\beta}u(p_2, \lambda_2), \quad (9)$$

$$\mathcal{M}_{5/2^\pm} = -\frac{g_{P_{cs}J/\psi}g_{P_{cs}KN}}{2M_{P_{cs}}m_Nm_{\Lambda}^2}\bar{u}(p_4, \lambda_4)\Gamma_{\nu}^{\mp}p_3^{\lambda}(p_3^{\mu}\epsilon^{*\nu}(p_3, \lambda_3) - \epsilon^{*\mu}(p_3, \lambda_3)p_3^{\nu})\frac{\Delta_{\mu\lambda\sigma\delta}}{s - M_{P_{cs}}^2}\epsilon^{\rho\sigma\alpha\beta}q_{\rho}\Gamma_{\alpha}^{\mp}p_{1\beta}p_1^{\delta}u(p_2, \lambda_2), \quad (10)$$

where  $\epsilon_{\mu}^*$  denotes the polarization vector for  $J/\psi$  and  $q$  stands for the momentum of  $P_{cs}$  given by  $q = p_1 + p_2 = p_3 + p_4$ . Taking into account the decay width of  $P_{cs}$ , we change the  $P_{cs}$  mass  $M_{P_{cs}}$  in the propagator to be  $(M_{P_{cs}} - i\Gamma_{P_{cs}}/2)$ . The spin projection operators for  $P_{cs}$  with spin 3/2 and 5/2 are defined respectively as [60]

$$\Delta_{\mu\sigma} = (\not{q} + M_{P_{cs}}) \left[ -g_{\mu\sigma} + \frac{1}{3}\gamma_{\mu}\gamma_{\sigma} + \frac{1}{3M_{P_{cs}}}(\gamma_{\mu}q_{\sigma} - \gamma_{\sigma}q_{\mu}) + \frac{2}{3M_{P_{cs}}^2}q_{\mu}q_{\sigma} \right],$$

$$\Delta_{\mu\lambda\sigma\delta} = (\not{q} + M_{P_{cs}}) \left[ \frac{1}{2}(\bar{g}_{\mu\sigma}\bar{g}_{\lambda\delta} + \bar{g}_{\mu\delta}\bar{g}_{\lambda\sigma}) - \frac{1}{5}\bar{g}_{\mu\lambda}\bar{g}_{\sigma\delta} - \frac{1}{10}(\bar{\gamma}_{\mu}\bar{\gamma}_{\sigma}\bar{g}_{\lambda\delta} + \bar{\gamma}_{\mu}\bar{\gamma}_{\delta}\bar{g}_{\lambda\sigma} + \bar{\gamma}_{\lambda}\bar{\gamma}_{\sigma}\bar{g}_{\mu\delta} + \bar{\gamma}_{\lambda}\bar{\gamma}_{\delta}\bar{g}_{\mu\sigma}) \right], \quad (11)$$

where

$$\bar{g}_{\mu\nu} = g_{\mu\nu} - \frac{q_{\mu}q_{\nu}}{M_{P_{cs}}^2}, \quad \bar{\gamma}_{\mu} = \gamma_{\mu} - \frac{q_{\mu}}{M_{P_{cs}}}\not{q}. \quad (12)$$

In the  $t$ -channel, we consider the exchange of the  $K$  and  $K^*$  mesons. The effective Lagrangians for the  $J/\psi KK$  and  $J/\psi KK^*$  vertices are given as

$$\begin{aligned}\mathcal{L}_{J/\psi KK} &= -ig_{J/\psi KK}\psi^\mu(K^+\partial_\mu K^- - K^-\partial_\mu K^+), \\ \mathcal{L}_{J/\psi KK^*} &= -\frac{g_{J/\psi KK^*}}{m_\psi}\epsilon^{\mu\nu\alpha\beta}\partial_\mu\psi_\nu K\partial_\alpha K_\beta^*,\end{aligned}\quad (13)$$

where  $m_\psi$  denotes the mass of  $J/\psi$ . The coupling constant will be determined by using a similar method as in the  $s$ -channel case. The decay amplitudes for the corresponding decays in Eq. (13) are obtained to be

$$\begin{aligned}A_{J/\psi KK} &= -g_{J/\psi KK}(q_K - q'_K)_\mu\epsilon^\mu, \\ A_{J/\psi KK^*} &= -\frac{g_{J/\psi KK^*}}{m_\psi}\epsilon^{\mu\nu\alpha\beta}q_{\psi\mu}q_{K^*\alpha}\epsilon_{\nu\beta}^*,\end{aligned}\quad (14)$$

where  $q'_K$  stands for the momentum of the kaon that goes to the opposite direction with  $q_K$ . The polarization vector of  $K^*$  is expressed by  $\epsilon_{K^*}^\mu$ . Since the decay widths of  $J/\psi$  to the  $K$  and  $K^*$  mesons are experimentally known as [56]

$$\begin{aligned}\Gamma_{J/\psi\rightarrow KK} &= 2.66 \times 10^{-2} \text{ keV}, \\ \Gamma_{J/\psi\rightarrow KK^*} &= 5.57 \times 10^{-1} \text{ keV},\end{aligned}\quad (15)$$

we can directly obtain the coupling constants  $g_{J/\psi KK}$  and  $g_{J/\psi KK^*}$ , respectively, as follows

$$g_{J/\psi KK} = 7.12 \times 10^{-4}, \quad g_{J/\psi KK^*} = 8.82 \times 10^{-3}.\quad (16)$$

Those for the  $\Lambda NK$  and  $\Lambda NK^*$  vertices are rather well known. The semiphenomenological nucleon-hyperon interaction such as the Nijmegen extended-soft-core model (ESC08a) [61] provides us with their values. Then, the effective Lagrangians for the  $\Lambda NK$  and  $\Lambda NK^*$  vertices are expressed as

$$\mathcal{L}_{\Lambda NK} = -\frac{f_{\Lambda NK}}{m_\pi}\bar{\Lambda}\gamma_\mu\gamma_5 N\partial^\mu K + \text{H.c.},\quad (17)$$

$$\begin{aligned}\mathcal{L}_{\Lambda NK^*} &= -g_{\Lambda NK^*}\bar{\Lambda}\gamma^\mu NK_\mu^* - \frac{f_{\Lambda NK^*}}{4m_N}\bar{\Lambda}\sigma^{\mu\nu}N(\partial_\mu K_\nu^* - \partial_\nu K_\mu^*) \\ &+ \text{H.c.},\end{aligned}\quad (18)$$

with the coupling constants given by

$$\begin{aligned}f_{\Lambda NK} &= -0.2643, & g_{\Lambda NK^*} &= -1.1983, \\ f_{\Lambda NK^*} &= -4.2386.\end{aligned}\quad (19)$$

Thus, the resulting transition amplitudes for  $K$  and  $K^*$  exchanges are respectively given as

$$\begin{aligned}\mathcal{M}_K &= \frac{g_{J/\psi KK}f_{\Lambda NK}}{m_\pi}\bar{u}(p_4, \lambda_4)\gamma_5 \\ &\times \frac{(2p_1 - p_3) \cdot \epsilon^*(p_3, \lambda_3)}{t - m_K^2}\not{q}_t u(p_2, \lambda_2),\end{aligned}\quad (20)$$

$$\begin{aligned}\mathcal{M}_{K^*} &= i\frac{g_{J/\psi KK^*}g_{\Lambda NK^*}}{m_\psi}\bar{u}(p_4, \lambda_4) \\ &\times \frac{\epsilon_{\mu\nu\alpha\beta}p_3^\mu\epsilon^{*\nu}(p_3, \lambda_3)q_t^\alpha}{t - m_{K^*}^2}\left(-g^{\beta\sigma} + \frac{q_t^\beta q_t^\sigma}{m_{K^*}^2}\right) \\ &\times \left(\gamma_\sigma + i\frac{\kappa_{K^*}}{2m_N}\sigma_{\gamma\sigma}q_t^\gamma\right)u(p_2, \lambda_2),\end{aligned}\quad (21)$$

where  $q_t = p_3 - p_1$  and  $\kappa_{K^*} = f_{\Lambda NK^*}/g_{\Lambda NK^*}$ .

As for the  $u$ -channel contribution, we consider only the  $N$  exchange. The effective Lagrangian for the  $NNJ/\psi$  vertex is similar to the  $P_{cs}$  with spin-1/2<sup>+</sup> as in Eq. (1)

$$\mathcal{L}_{J/\psi NN} = -g_{J/\psi NN}\bar{N}\gamma_\mu\psi^\mu N - \frac{f_{J/\psi NN}}{2M_N}\bar{N}\sigma_{\mu\nu}\psi^{\mu\nu}N + \text{H.c.}\quad (22)$$

Since the  $J/\psi$  vector meson has a nature similar to the  $\phi$  vector meson, we ignore the second term with the tensor coupling constant, since its value is related to the charmed magnetic moment of the nucleon, which can be neglected. It is also difficult to determine the vector coupling constant  $g_{J/\psi NN}$ . We take its value from Ref. [62]:  $g_{J/\psi NN} = g_{J/\psi N\bar{N}} = 1.62 \times 10^{-3}$ . This small value indicates already that the  $u$ -channel contribution will be very tiny. The corresponding  $u$ -channel amplitude is obtained as

$$\begin{aligned}\mathcal{M}_N &= -\frac{g_{J/\psi NN}f_{\Lambda NK}}{m_\pi}\bar{u}(p_4, \lambda_4)\gamma_5\not{p}_1 \\ &\times \frac{\not{q}_u + m_N}{u - m_N^2}\not{q}^*(p_3, \lambda_3)u(p_2, \lambda_2),\end{aligned}\quad (23)$$

where  $q_u = p_4 - p_1$ .

Since hadrons have finite sizes and structures, it is essential to consider a form factor at each vertex. Actually, there is no firm theoretical ground as to how one can determine the values of the cutoff masses. In practice, the values of the cutoff masses are usually fitted to the experimental data. Unfortunately, we do not have experimental data enough to determine them in the present case. Nevertheless, there is one theoretical guideline. As discussed in Ref. [63], heavier baryons are considered to be more compact than lighter ones, which was found by examining the electromagnetic form factors of singly heavy baryons. By “*more compact*” we mean that the intrinsic size of the heavier baryons (or hadrons) should be smaller than the light ones, which leads to larger values of the cutoff masses in general. Being guided by this, we have chosen the cutoff masses  $\Lambda$  in such a way that  $\Lambda - m \simeq 600\text{--}700$  MeV. In the present work, we will take the form factors, which are most used in reaction calculations. So, we introduce the form factors in the  $s$ -,  $t$ - and  $u$ -channels, respectively, as follows:

$$\begin{aligned}
 F_s(q^2) &= \frac{\Lambda^4}{\Lambda^4 + (s - m^2)^2}, \\
 F_t(q_t^2) &= \frac{\Lambda^2 - m^2}{\Lambda^2 - t}, \\
 F_u(q_u^2) &= \frac{\Lambda^2 - m^2}{\Lambda^2 - u},
 \end{aligned} \tag{24}$$

with the values of the cutoff masses taken to be

$$\begin{aligned}
 \Lambda_{P_{cs}} &= 5.0 \text{ GeV}, & \Lambda_K &= 1.0 \text{ GeV}, \\
 \Lambda_{K^*} &= 1.4 \text{ GeV}, & \Lambda_N &= 1.5 \text{ GeV}.
 \end{aligned} \tag{25}$$

Note that these values of the cutoff masses have been used in various different reactions.

### B. Regge approach

The effective Lagrangian method is known to describe well the hadronic productions at low-energy regions, in particular, in the vicinity of the threshold energy. However, since this method is based on the Born approximation, i.e., a tree-level calculation, it is not suitable to explain the exclusive or diffractive hadronic processes at higher energies. On the other hand, the Regge approach explains the general high-energy behaviors of the hadronic reactions but only qualitatively. To overcome this disadvantage, a hybridized Regge approach was phenomenologically proposed [48] in an attempt to improve the Regge approach quantitatively. This approach is characterized by replacing the Feynman propagator derived from the effective Lagrangian method by the Regge one

$$\frac{1}{t - m_X^2} \rightarrow \mathcal{P}_{\text{Regge}}^\pm = -\Gamma(-\alpha_X(t)) \xi_X^\pm \alpha'_X \left( \frac{s}{s_0} \right)^{\alpha_X(t)}. \tag{26}$$

This method was successfully applied to hadronic reactions throughout broad energy regions including even the resonance regions,  $\sqrt{s} \sim 3 \text{ GeV}$  [42,43].

#### 1. $K$ and $K^*$ Reggeon exchange

In Fig. 2, we depict schematically the  $t$ -channel diagram in terms of the quark lines [46]. As shown in Fig. 2, hadronic  $J/\psi$  productions by the photon,  $\pi$  or  $K$  beams are all OZI suppressed, being similar to the  $\phi$ -meson production. So, we consider the light-Reggeon exchanges in the  $t$ -channel, i.e., the  $K$  and  $K^*$  Reggeons. We employ here a hybridized Regge method, in which the Feynman propagators in the transition amplitudes obtained in the previous subsection are replaced by the Regge propagator [44,48,64,65]. Thus, we can express the transition amplitudes with the  $K$ - and  $K^*$ -Reggeon exchanges, respectively, as

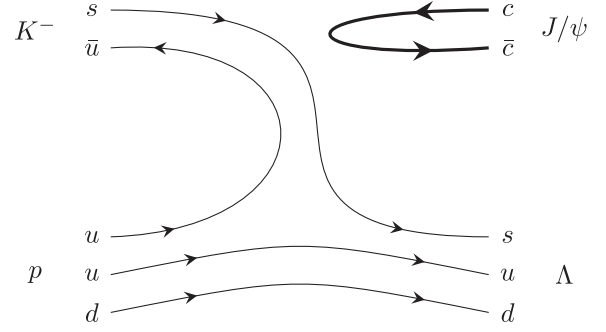


FIG. 2. The  $t$ -channel schematic diagram for the hidden-charm  $Kp \rightarrow J/\psi\Lambda$  reaction.

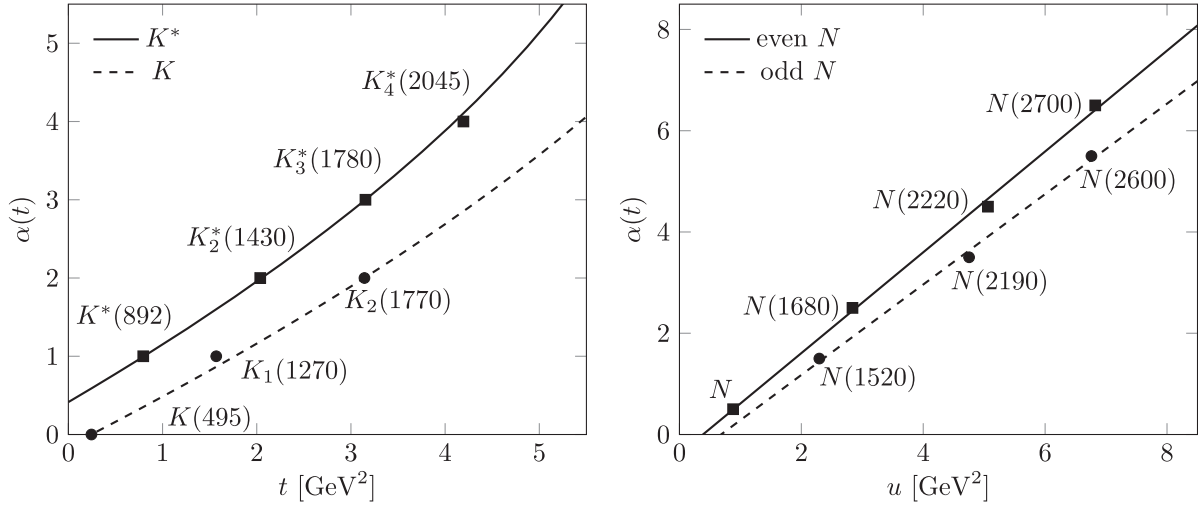
$$\begin{aligned}
 \mathcal{M}_K^R(s, t) &= -\mathcal{M}_K(s, t) \left\{ \frac{1}{e^{-i\pi\alpha_K(t)}} \right\} \\
 &\times \Gamma(-\alpha_K(t)) \alpha'_K(m_K^2) \left( \frac{s}{s_0} \right)^{\alpha_K(t)} (t - m_K^2),
 \end{aligned} \tag{27}$$

$$\begin{aligned}
 \mathcal{M}_{K^*}^R(s, t) &= -\mathcal{M}_{K^*}(s, t) \left\{ \frac{1}{e^{-i\pi\alpha_{K^*}(t)}} \right\} \\
 &\times \Gamma(1 - \alpha_{K^*}(t)) \alpha'_{K^*}(m_{K^*}^2) \left( \frac{s}{s_0} \right)^{\alpha_{K^*}(t)-1} (t - m_{K^*}^2),
 \end{aligned} \tag{28}$$

where  $\alpha_K$  and  $\alpha_{K^*}$  denote the Regge trajectories for the  $K$  and  $K^*$  mesons, respectively.  $\alpha'(t)$  represents the derivative of  $\alpha$  with respect to  $t$ :  $\alpha'(t) = \partial\alpha/\partial t$ . The scale parameter  $s_0$  is a free parameter. Though this can be fitted to the data, if they exist, its value is widely taken to be  $s_0 = 1 \text{ GeV}^2$ , which corresponds to a typical hadronic scale. This can be also estimated theoretically. If the  $t$ -channel diagram as shown in Fig. 2 were a planar diagram, the energy-scale parameter  $s_0$  could have been calculated by using the planar diagram decomposition [66,67]. However, the  $t$ -channel diagram for the  $K^-p \rightarrow J/\psi\Lambda$  reaction is not a planar one. So, there is no clear way to determine the value of  $s_0$ . In the present work, we will utilize the result of Model I as a guideline to determine  $s_0$ . Since the Regge amplitude have to be consistent with that of Model I at the Regge pole position, we extract the value of  $s_0$  by comparing the results for the  $d\sigma/dt$  from Model I with those for Model II near the pole. The reasonable values of  $s_0$  turn out to be  $s_0 = 5 \text{ GeV}^2$  for  $K^-$ - and  $s_0 = 2 \text{ GeV}^2$  for  $K$ -Reggeon exchange.

Though the linear Regge trajectories are given, we will adopt the nonlinear Regge trajectories [68], since it describes the trajectories more realistically as shown in Fig. 3. Thus,  $\alpha_K$  and  $\alpha_{K^*}$  are parametrized as

$$\alpha_{K(K^*)}(t) = \alpha_{K(K^*)}(0) + \gamma \left( \sqrt{T_{K(K^*)}} - \sqrt{T_{K(K^*)} - t} \right), \tag{29}$$


 FIG. 3. Regge trajectories for  $K$ ,  $K^*$  and nucleon.

where  $\gamma$  governs the slope of the trajectories and  $T_{K(K^*)}$  denote their terminal points. The parameters for the  $K$  and  $K^*$  trajectories are fixed to be

$$\gamma = 3.65 \text{ GeV}^{-1}, \quad \alpha_K(0) = -0.151, \quad \alpha_{K^*}(0) = 0.414, \\ \sqrt{T_K} = 2.96 \text{ GeV}, \quad \sqrt{T_{K^*}} = 2.58 \text{ GeV}. \quad (30)$$

Note that in the limit  $t \rightarrow 0$ , this square-root trajectory reduces to the linear function

$$\alpha(t) \approx \alpha(0) + \frac{\gamma}{2\sqrt{T}} t = \alpha(0) + \alpha'(0)t. \quad (31)$$

Before we carry out the numerical calculation, it is of great interest to examine the asymptotic behavior of the differential cross section  $d\sigma/dt$ . It is known that in the large  $s$  limit the asymptotic behavior of  $d\sigma/dt$  is given as

$$\frac{d\sigma}{dt}(s \rightarrow \infty, t \rightarrow 0) \propto s^{2\alpha(0)-2}. \quad (32)$$

We found that the transition amplitudes are proportional to  $t$  and  $s$  as follows

$$\lim_{s \rightarrow \infty} \sum_{\lambda_i, \lambda_f} |\mathcal{M}_{K^*}(t - m_{K^*}^2)|^2 \propto s^2 t \quad (33)$$

and the differential cross section

$$\frac{d\sigma}{dt} = \frac{1}{64\pi s} \frac{1}{|p_{\text{cm}}|^2} \sum_{\lambda_i, \lambda_f} |\mathcal{M}_{K^*}^R|^2 \\ \propto \sum_{\lambda_i, \lambda_f} |\mathcal{M}_{K^*}(t - m_{K^*}^2)|^2 s^{2\alpha(t)-4} \propto_{s \rightarrow \infty} s^{2\alpha(t)-2}, \quad (34)$$

which reproduces correctly the asymptotic behavior given in Eq. (32). Here,  $p_{\text{cm}}$  stands for the initial momentum in

the CM frame, which is proportional to  $\sqrt{s}$  in the large  $s$  limit. The numerical results for  $d\sigma/dt$  with  $K$  and  $K^*$  considered only are depicted in Fig. 4. As one can see already in Eq. (33), the contribution of  $K^*$  exchange to  $d\sigma/dt$  decreases rapidly at very forward scattering  $t \rightarrow 0$  in the same context of  $\gamma N \rightarrow K\Lambda$  [48] and  $\pi N \rightarrow K^*\Lambda$  [43] reactions. As  $t$  increases,  $d\sigma/dt$  falls off linearly for  $K$  exchange, whereas that for  $K^*$  exchange grows very fast in the forward direction, and then decreases almost linearly.

As shown in the left panel of Fig. 3, the even and odd signed  $K$  ( $K^*$ ) poles are lying on the same trajectory, which means that the  $K$  ( $K^*$ ) Regge trajectory is *degenerate*. When the total transition amplitudes are derived, the even and odd Regge propagators can be added or subtracted [48,69]. Thus, the Regge propagator for  $K$  ( $K^*$ ) thus contains either 1 (constant phase) or  $e^{-i\pi\alpha(t)}$  (rotating phase). However, we find that the results for the total and differential cross sections are not much changed by the signature factor, so we choose the constant signature factor. On the other hand, note that the asymmetry will be quite sensitive to this factor, which will not be computed in the present work.

## 2. $N$ Reggeon exchange

We will follow the same method for the nucleon Reggeon in the  $u$ -channel. Replacing the Feynman propagator by the Regge propagator, we obtain the transition amplitudes for the  $u$ -channel as follows

$$\mathcal{M}_R(s, u) = -\mathcal{M}_N(s, u) \xi_N^+ \Gamma(0.5 - \alpha_N(u)) \\ \times \alpha'_N \left( \frac{s}{s_0} \right)^{\alpha_N(u)-0.5} (u - m_N^2). \quad (35)$$

We take the linear trajectory as in Ref. [70]. Based on the nucleon trajectory drawn in the right panel of Fig. 3, we

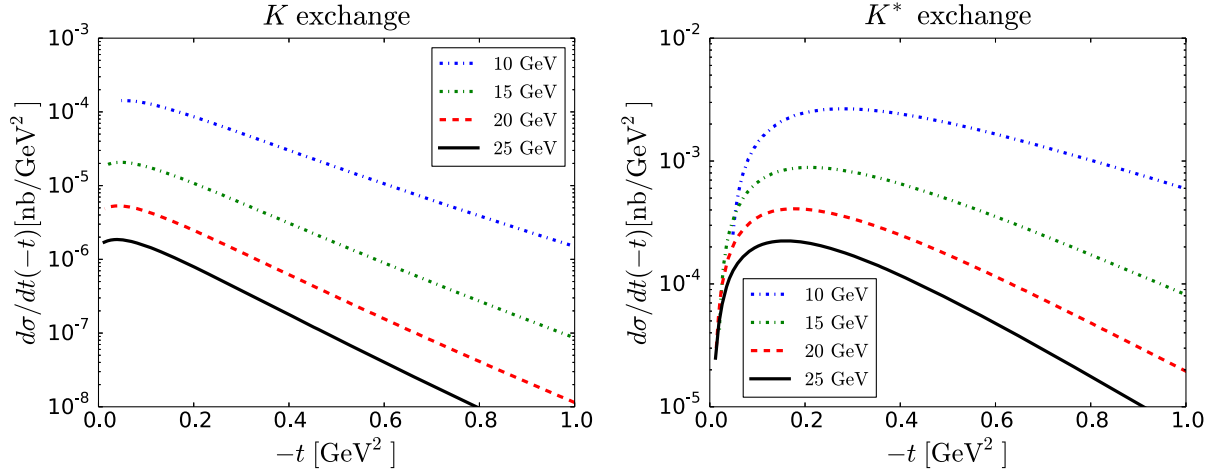


FIG. 4.  $d\sigma/dt$  as a function of  $-t$  for the  $K$  and  $K^*$  contributions from  $W = 10$  GeV to 25 GeV.

find the Regge trajectory for the even signured nucleon [56] as

$$\alpha_N(u) = \alpha_N(0) + \alpha'_N u; \quad \alpha_N(0) = -0.384, \quad \alpha'_N = 0.996. \quad (36)$$

Since one can distinguish the even and odd  $N$  trajectory for the nucleon, so the signature factor for the nucleon Regge trajectory can be taken to be

$$\xi_N^+ = \frac{1 + e^{-i\pi\alpha_N(u)}}{2}. \quad (37)$$

The energy-scale parameter  $s_0$  cannot be obtained by using the similar way as in the  $t$ -channel because of the following reason. It is related to the asymptotic behavior of the  $u$ -channel Regge propagator. At very high energy and in the very forward direction, which correspond to  $s \rightarrow \infty$  and  $t \rightarrow 0$ , respectively, we get  $u \approx -s$  that leads to  $\alpha(u) \approx -\alpha's$ . Moreover, using the asymptotic behavior of the  $\Gamma$  function when  $z \rightarrow \infty$ , we find an approximated relation

$$\Gamma(z) \approx \sqrt{2\pi(z-1)} \left( \frac{z-1}{e} \right)^{z-1}. \quad (38)$$

Thus, Eq. (35) is reduced to

$$\mathcal{M}_R(s \rightarrow \infty, u \approx -s) \approx \mathcal{M}_F(s, u) C s^\beta (\alpha'_N s_0 / e)^{\alpha'_N s}. \quad (39)$$

The last factor in Eq. (39) gives a hint on  $s_0$ . If  $\alpha's_0 > e$ , then the above given amplitude will diverge as  $s$  grows. Since  $\alpha'_N$  is less than 1, we are able to fix the energy-scale parameter to be  $s_0 = 2$  GeV<sup>2</sup> such that the amplitude is kept to be convergent.

### III. RESULTS AND DISCUSSION

We first examine each contribution to the total cross section. In Fig. 5, we show the results for each contribution to the total cross section for the  $K^- p \rightarrow J/\psi \Lambda$  reaction. We consider here the hidden-charm pentaquark  $P_{cs}$  with  $J^P = 1/2^-$  and  $J^P = 3/2^-$  in the  $s$  channel. The resonance peak reaches the magnitude of nb order, i.e.,  $\sigma \sim 1$  nb at  $W \approx 4.46$  GeV. The contribution from  $K^*$  exchange in the  $t$  channel is the most dominant one apart from the resonance region. Those from  $K$  and  $N$  exchanges are negligibly small, since they are approximately 100 times

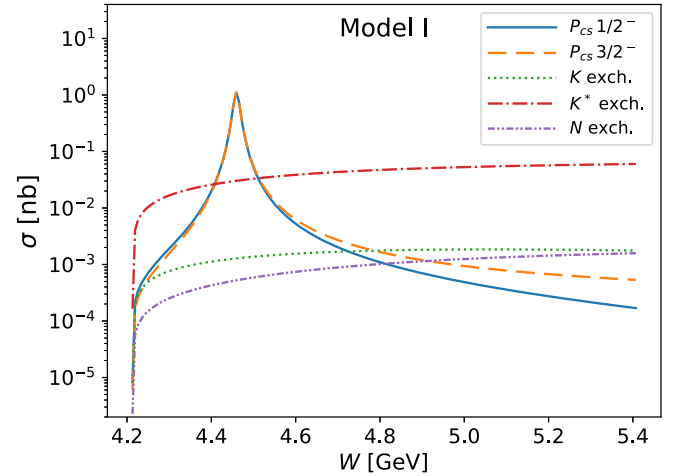


FIG. 5. Numerical results for the total cross section as a function of the total CM energy ( $W$ ) from Model I. We consider two different cases of spin-parity quantum number for  $P_{cs}$ , i.e.,  $J^P = 1/2^-$  and  $J^P = 3/2^-$ . The  $s$ -channel contribution is drawn in the solid and dashed curves in the case of  $J^P = 1/2^-$  and  $J^P = 3/2^-$ , respectively. The dot-dashed curve depicts the contribution from  $K^*$  exchange in the  $t$  channel, whereas the dotted one illustrates that from  $K$  exchange. The two-dot-dashed one draws the contribution from  $N$  exchange in the  $u$  channel.

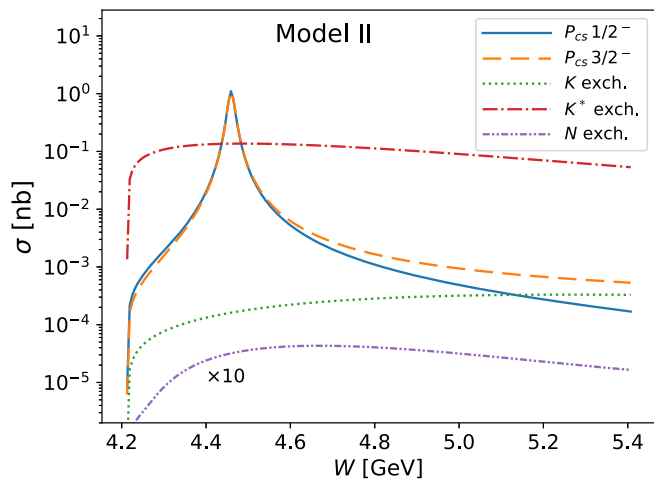


FIG. 6. Numerical results for the total cross section as a function of the total CM energy ( $W$ ) from Model II. Notations are the same as in Fig. 5.

smaller than the contribution from  $K^*$  exchange. The reason can be found from the difference in the values of the coupling constants, given in Eq. (16). The coupling constant for the  $J/\psi KK^*$  vertex is at least ten times larger than that for the  $J/\psi KK$  vertex. Thus, the contribution from  $K^*$  exchange to the total cross section is much larger than those from both  $K$  and  $N$  exchanges.

In Fig. 6, we draw the results for each contribution, which are obtained from Model II, i.e., from the Regge approach. Since the  $s$ -channel diagram is simply the same as that from Model I, we discuss the contributions from  $K^*$ ,  $K$ , and  $N$  exchanges. As mentioned previously, the value of the energy-scale parameter  $s_0$  is important for the size of the transition amplitudes. Since we use the results from Model I as a guiding principle for determining  $s_0$ , we expect that the magnitudes of the  $K^*$ - and  $K$ -Reggeon contributions should be comparable to those from Model I. However,  $s_0$  in the Regge transition amplitude for  $N$ -Reggeon exchange

in the  $u$  channel is constrained by the convergence condition. This means that the effect of  $N$  exchange is extremely small, so that we can even ignore it. Comparing the results from Model II, we find that the  $K^*$  contributions from Model I exhibit different dependence on  $W$ . It is known from the asymptotic behavior of the differential cross sections shown in Eq. (34) that the contributions of  $K$ - and  $K^*$ -Reggeon exchanges should fall off slowly as  $W$  increases. As depicted in Fig. 6,  $K^*$ -Reggeon contribution indeed decreases as  $W$  increases. On the other hand, the results for  $K^*$  exchange in Model I slowly increase as  $W$  increases. This implies that the effective Lagrangian method is limited in describing hadronic processes at higher energies, though it is a very effective method in the vicinity of the threshold. The contribution of  $K$ -Reggeon exchange seems to arise as  $W$  increases. However, if one further increases  $W$ , the contribution of  $K$ -Reggeon exchange starts to fall off.

In Fig. 7, we will examine the dependence of the results for the total cross section on the values of the branching ratio of the  $P_{cs} \rightarrow J/\psi\Lambda$  decay. As expected, if the value of the branching ratio increases, the peak corresponding to  $P_{cs}$  is enhanced clearly. Interestingly, the size of the peak reaches approximately 10 nb when  $\text{Br}(P_{cs} \rightarrow J/\psi\Lambda) = 10\%$  is used. When  $\text{Br}(P_{cs} \rightarrow J/\psi\Lambda) = 50\%$  is employed,  $\sigma$  is obtained to be almost 100 nb in the vicinity of the resonance. This implies that if  $\text{Br}(P_{cs} \rightarrow J/\psi\Lambda)$  is larger than 10%, then  $P_{cs}$  would have been already found in the data for  $K^-p$  scattering. Thus, the 1% branching ratio is a quite reasonable one, which is in agreement with that from Refs. [26,59].

The spin-parity quantum number for  $P_{cs}^0(4459)$  is experimentally unknown yet. While it may have favorably either  $J^P = 1/2^-$  or  $J^P = 3/2^-$ , it is of great interest whether one can see how the total cross sections and other observables for the  $K^-p \rightarrow J/\psi\Lambda$  reaction can provide a hint on the spin-parity quantum number for  $P_{cs}$ . If the final states consisting of  $J/\psi$  and  $\Lambda$  in the  $S$  wave, the spin-parity quantum numbers  $J^P = 1/2^-$  and  $J^P = 3/2^-$  of  $P_{cs}$  will be

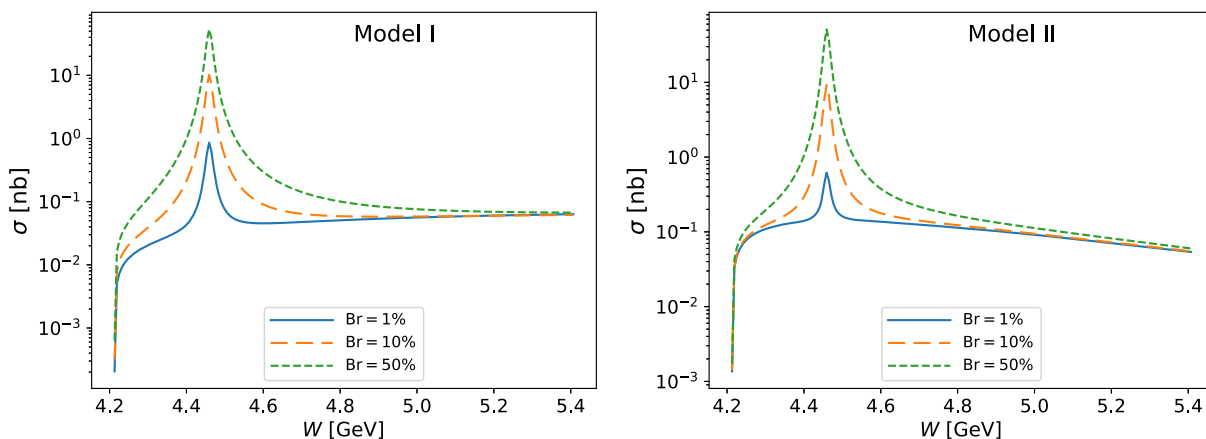


FIG. 7. Numerical results for the total cross section as a function of the total CM energy ( $W$ ) from Model I (left panel) and Model II (right panel) with the branching ratio  $B(P_{cs} \rightarrow J/\psi\Lambda)$  varied in the range of (1 – 50)%.

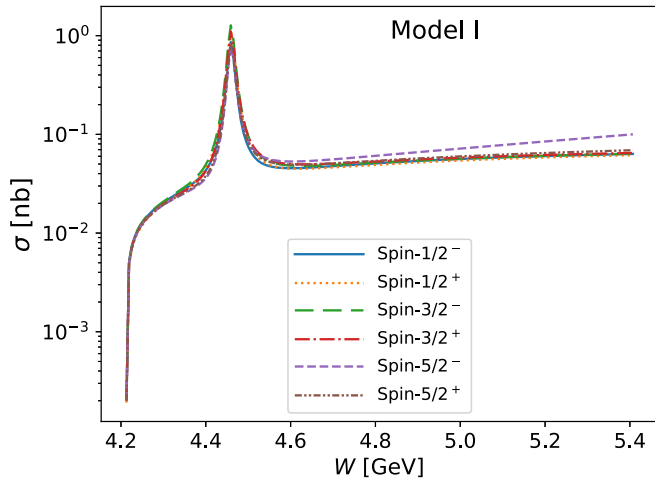


FIG. 8. Numerical results for the total cross section as a function of the total CM energy ( $W$ ) from Model I with possible  $J^P$  quantum numbers employed. Six different combinations of the spin and parity for the hidden-charm strange pentaquark  $P_{cs}$  are taken into account.

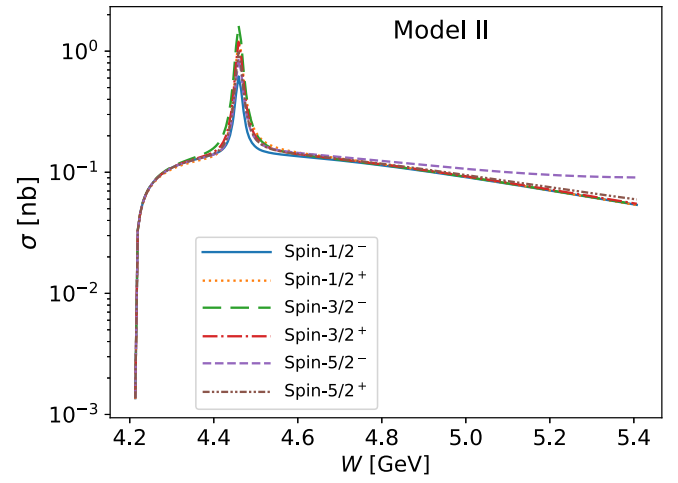


FIG. 9. Numerical results for the total cross section as a function of the total CM energy ( $W$ ) from Model II with possible  $J^P$  quantum numbers employed. Six different combinations of the spin and parity for the hidden-charm strange pentaquark  $P_{cs}$  are taken into account.

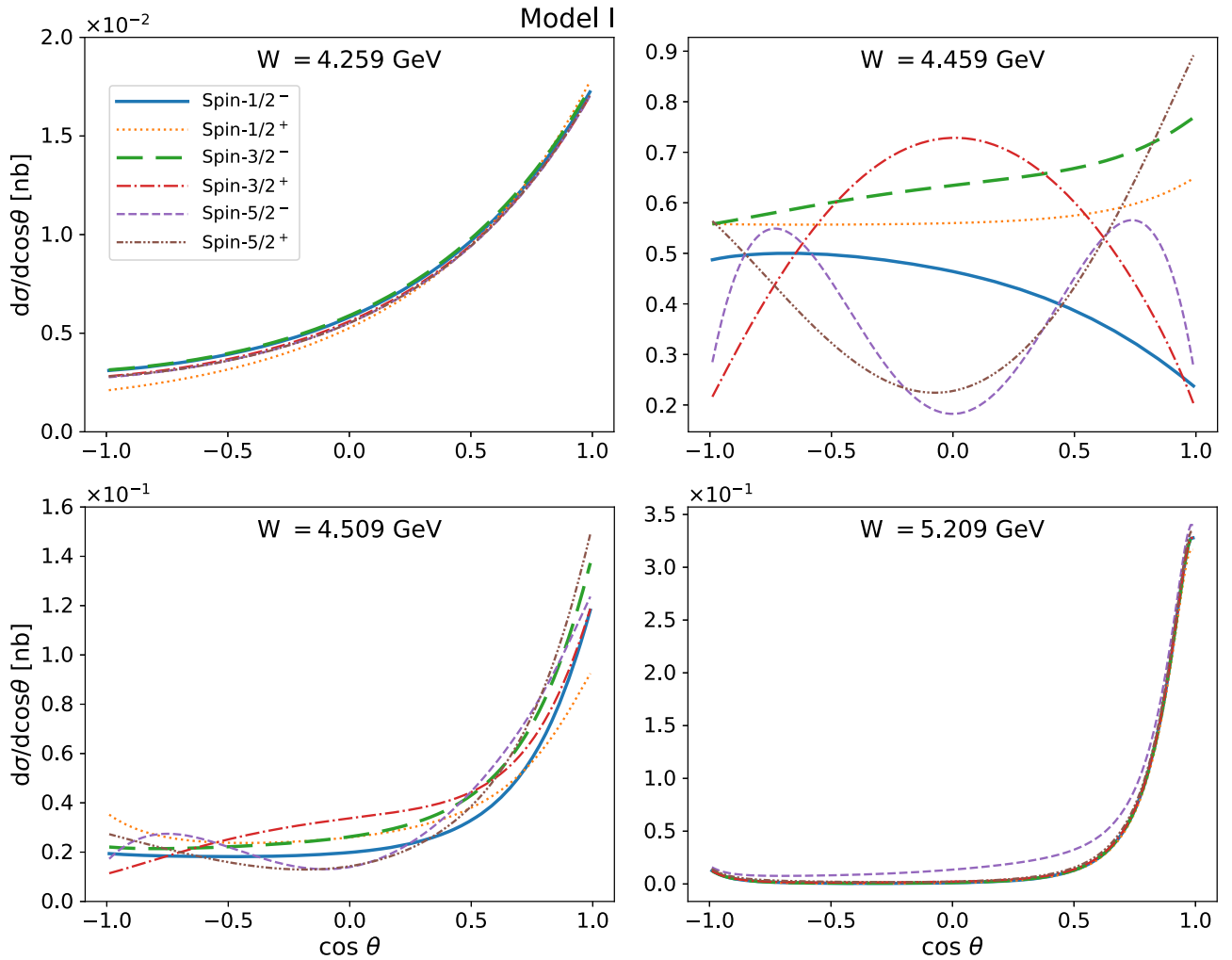


FIG. 10. Results for the differential cross sections ( $d\sigma/d\cos\theta$ ) as functions of  $\cos\theta$  for a given total energy ( $W$ ) from Model I. The notation of the curves is the same as in Fig. 8.

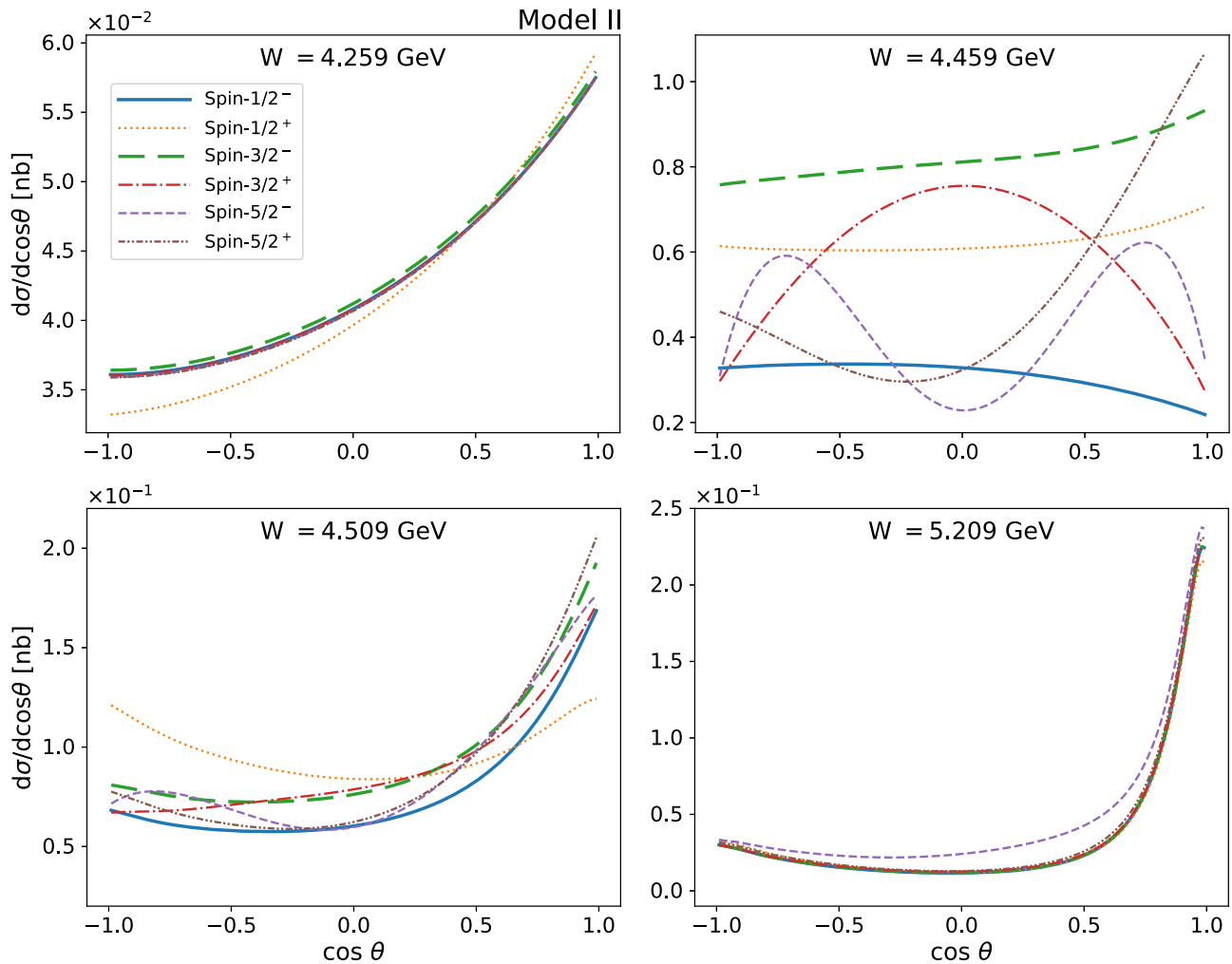


FIG. 11. Results for the differential cross sections ( $d\sigma/d\cos\theta$ ) as functions of  $\cos\theta$  for a given total energy ( $W$ ) from Model II. The notation of the curves is the same as in Fig. 8.

favored. However, there is no reason to reject other states with higher values of the orbital angular momentum. Thus, we consider six different combinations for the spin and parity for  $P_{cs}$ , i.e.,  $J^P = 1/2^-, 1/2^+, 3/2^-, 3/2^+, 5/2^-,$  and  $5/2^+$ . In Figs. 8 and 9, we draw the results for the total cross sections by considering the six different combinations of the spin-parity quantum numbers for  $P_{cs}$ , using Model I and Model II, respectively. We find that except for the case of  $J^P = 5/2^-$ , all the results seem very similar each other. While the result for  $J^P = 5/2^-$  from Model I shows a similar behavior in the resonance region, it increases monotonically faster than all the other cases as  $W$  increases. On the other hand, the results from Model II decrease monotonically as  $W$  increases again except for the  $J^P = 5/2^-$  case. Even the total cross section for  $P_{cs}(J^P = 5/2^-)$  will decrease, if  $W$  further increases, though we did not show it in Fig. 9.

Figures 10 and 11 depict the numerical results for the differential cross sections  $d\sigma/d\cos\theta$  as functions of  $\cos\theta$  with four different values of  $W$  given. The results

near the threshold ( $W = 4.259$  GeV) clearly show that the magnitudes of the differential cross sections in the forward direction are the largest ones and then decrease monotonically as  $\cos\theta$  goes from  $+1$  to  $-1$ . So, the results for the differential cross sections are mostly diminished in the backward direction. While the results from Model II at  $W = 4.259$  GeV exhibit similar behaviors to those from Model I, detailed dependences on  $\cos\theta$  look different.

When it comes to the resonance region at  $W = 4.459$  GeV, the results are noticeably distinguished for different assignments of  $J^P$  to  $P_{cs}$ . Scrutinizing first the results for the cases of  $J^P = 1/2^-$  and  $J^P = 3/2^-$ , we find that the  $\cos\theta$  dependence of them is rather different. The result for  $P_{cs}^0(J^P = 1/2^-)$  is suppressed in the forward direction, whereas that for  $P_{cs}^0(J^P = 3/2^-)$  gets enhanced as  $\cos\theta$  increases. This implies that the resonance and the  $K^*$  exchange contributions interfere differently each other. When  $J^P = 1/2^-$  is assumed, the two terms interfere destructively, while they do constructively with

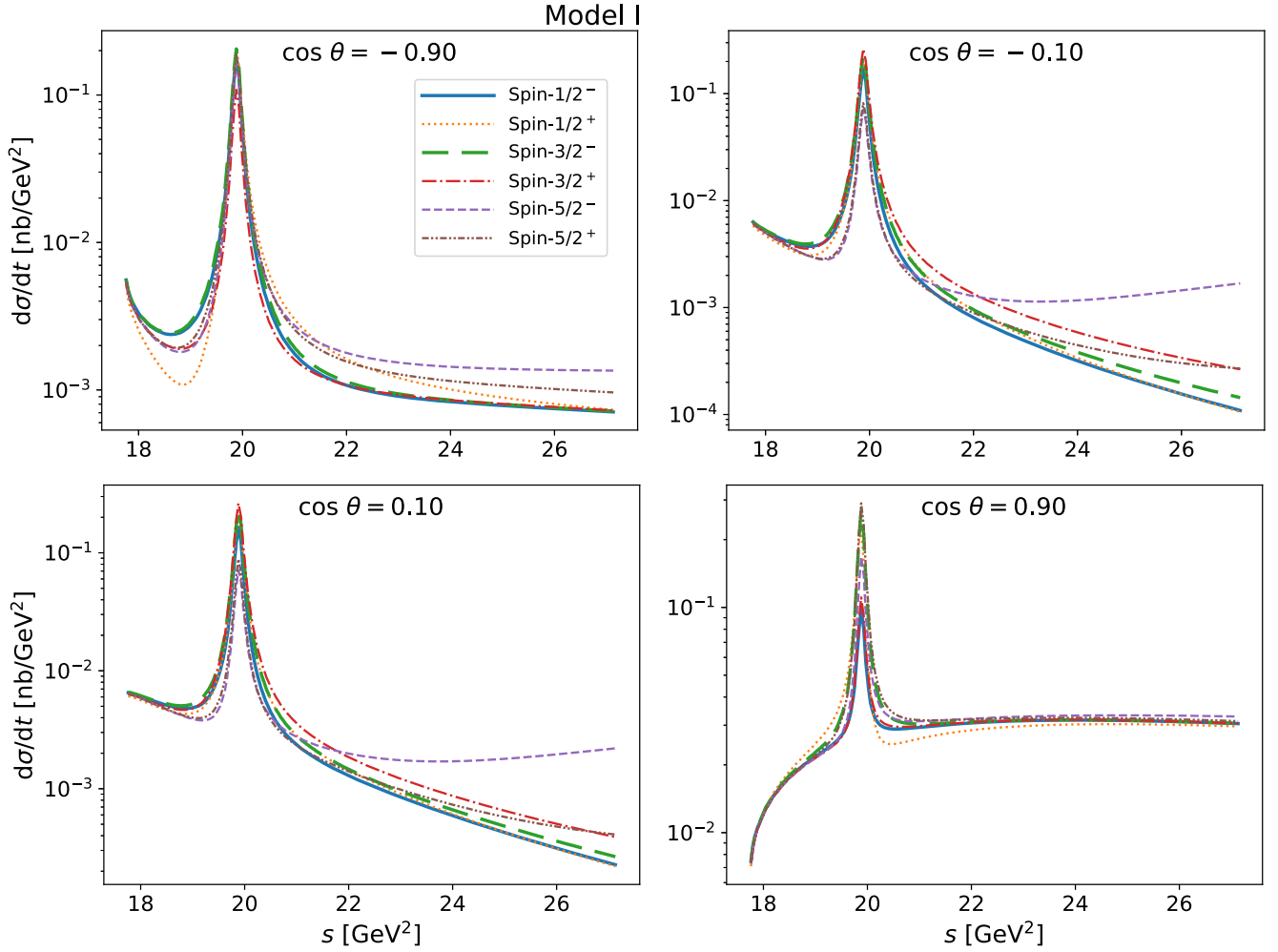


FIG. 12. Results for the differential cross sections ( $d\sigma/d\cos\theta$ ) as functions of  $s$  for a given angle ( $\cos\theta$ ) from Model I. The notation of the curves is the same as in Fig. 8.

$J^P = 3/2^-$  assumed. When one takes  $J^P = 3/2^+$  for  $P_{cs}$ , the corresponding differential cross section becomes maximum at  $\cos\theta = 0$ , i.e.,  $\theta = 90^\circ$ . On the other hand, if  $J^P = 5/2^+$  is assumed, the values of the differential cross section will be the minimum at  $\theta = 90^\circ$ . When  $J^P = 5/2^-$  is imposed, the result for  $d\sigma/d\cos\theta$  becomes more complicated. Thus, the measurement of the differential cross sections near the resonance region may provide one way of determining the spin-parity quantum numbers for  $P_{cs}$  in the  $K^-p \rightarrow J/\psi\Lambda^0$  reaction.

In Figs. 12 and 13, we depict the results for the differential cross sections  $d\sigma/dt$  as functions of  $W$ , which are obtained from Model I and II, respectively, varying the scattering angle  $\cos\theta$  from  $\cos\theta = 0.9$  to  $\cos\theta = -0.9$ . In the forward direction, the results for  $d\sigma/dt$  look similar to those for the total cross sections. However, the results at  $\cos\theta = 0.1$  and  $\cos\theta = -0.1$  enable us to distinguish among those with different  $J^P$ . While the shapes of the resonances corresponding to  $P_{cs}$  look all similar, one can distinguish them each other as

increases. Getting out of the resonance regions, the results decrease as  $s$  increases except for the case of  $J^P = 5/2^-$ , in particular, when one uses Model I. In fact, we already found this behavior in the results for the total differential cross sections. However, we can see this particular behavior more prominently in those for  $d\sigma/dt$  as  $s$  increases. The reason is clear. As shown in Eqs. (8), (9), and (10), the transition amplitudes contain strong momentum dependence with higher spin of  $P_{cs}$  assumed. As  $s$  further increases, the results for  $J^P = 5/2^+$  also start to increase slowly. This comes from the fact that the difference in the parity also affects the interference effects. Moreover, this peculiar dependence of  $d\sigma/dt$  for  $J^P = 5/2^-$  on  $s$  implies that the effective Lagrangian method may not be valid anymore at very high energies. On the other hand, the Regge approach nicely produces the asymptotic behavior of  $d\sigma/dt$  as  $s$  increases. Even the result for  $d\sigma/dt$  with  $J^P = 5/2^-$  assigned starts to fall off when  $s$  further increases, though we do not show in Fig. 13 explicitly.

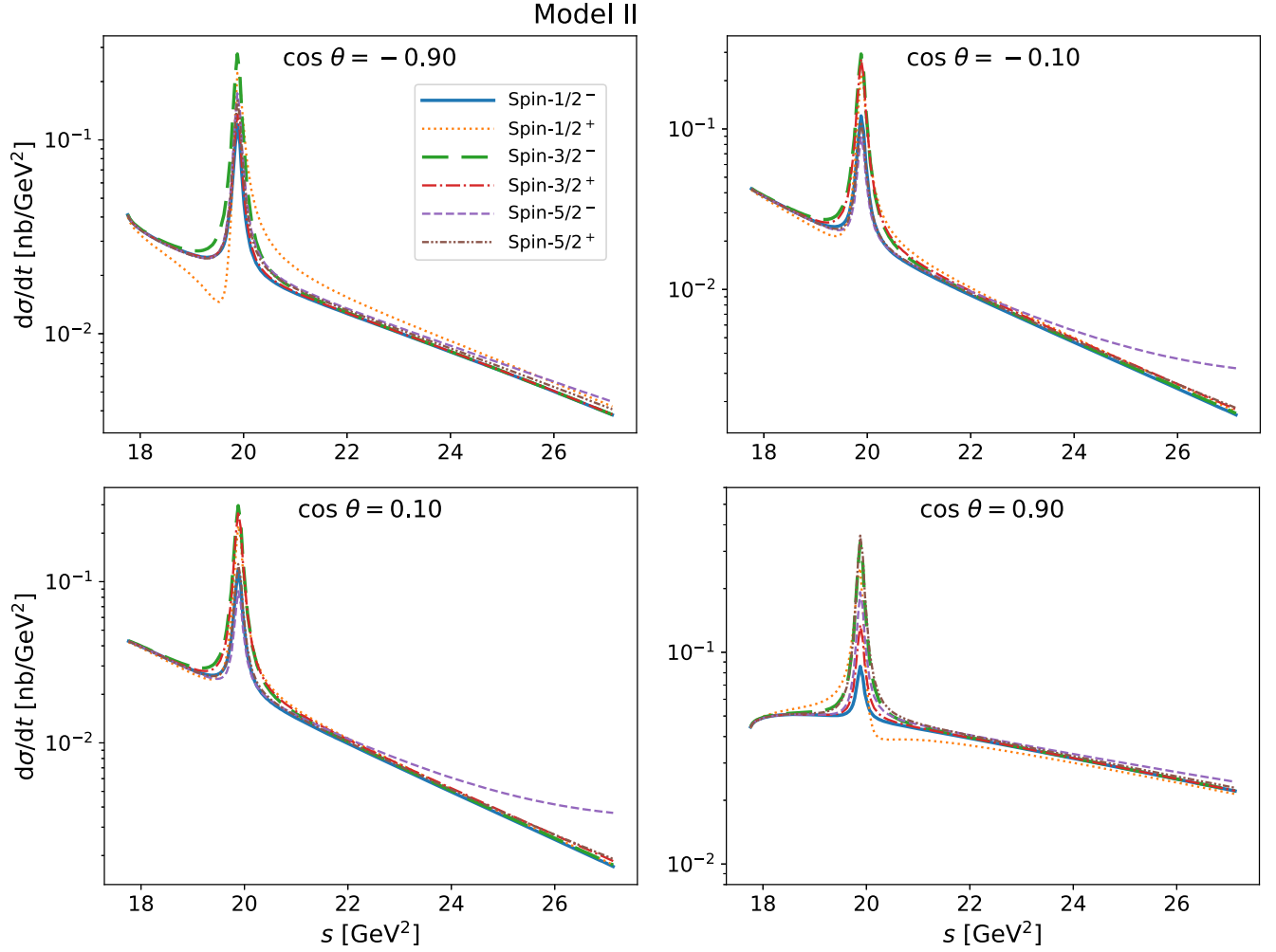


FIG. 13. Results for the differential cross sections ( $d\sigma/d\cos\theta$ ) as functions of  $s$  for a given angle ( $\cos\theta$ ) from Model II. The notation of the curves is the same as in Fig. 8.

#### IV. SUMMARY AND CONCLUSION

In the present work, we aimed at investigating the production of  $P_{cs}^0(4459)$  in the  $K^-p \rightarrow J/\psi\Lambda^0$  reaction, employing two different theoretical frameworks, i.e., the effective Lagrangian method and the Regge approach. We call these two different approaches as Model I and Model II, respectively. We first determined the coupling constants for all the relevant hadronic vertices. Since there is lack of experimental data on them, we made various reasonable assumptions. To determine the coupling constant for the  $P_{cs}J/\psi\Lambda$  vertex, we assumed that the branching ratio of  $P_{cs} \rightarrow J/\psi\Lambda$  decay is about 1%. That of  $P_c \rightarrow J/\psi N$  was also proposed to be about 0.01%. Thus, the coupling constant  $g_{P_{cs}J/\psi\Lambda}$  is of order 0.1. When one considers the hidden-charm pentaquark with higher spins ( $J^P \geq 3/2^\pm$ ), the tensor couplings are naturally introduced. However, since  $J/\psi$  is an isosinglet, the tensor coupling constants can be neglected as in the case of the  $\omega$  meson. Moreover, since we are mainly interested in the resonance

$P_{cs}$  region, which is not far from the threshold of  $J/\psi$  and  $\Lambda$ , the contributions from the tensor couplings can be taken to be very small. Since the Okubo-Zweig-Iizuka rule indicates that the coupling between a nucleon and a  $\phi$  meson ( $s\bar{s}$ ) should be very small, the same is applied to the coupling between a hyperon and a charmonium ( $c\bar{c}$ ). Thus, we also took the value of the coupling constant for the  $KP_{cs}N$  vertex to be very small. By estimating the branching ratio of  $P_{cs} \rightarrow K^-p$ , we found that the value of the  $KP_{cs}N$  coupling constant is of order  $10^{-3}$ .

Since the decay widths of  $J/\psi$  to the  $K$  and  $K^*$  mesons are known, we were able to determine directly the corresponding coupling constants from experimental data. Our results are obtained by setting the cut-off mass for the off-shell  $P_{cs}$  to 5 GeV, which is a rather plausible choice, even if we observe that our predictions are extremely sensitive to the value of the cutoff, which means that if one can change the value a little bit, then the results would be very much changed. On the other hand, since there are no experimental

data to determine the values of the cutoff masses certain uncertainties caused by them are inevitable. As for the form factors for  $K$  and  $K^*$ , we fixed the values of the cutoff masses to be  $\Lambda_K = 1$  GeV and  $\Lambda_{K^*} = 1.4$  GeV. In the case of the Regge approach, we considered a nonlinear form of the  $K$  and  $K^*$  Regge trajectories, which fit the experimental data much better than the linear ones.

We first scrutinized the results for the total cross sections as functions of the CM total energy  $W$ , with different spin-parity quantum numbers  $J^P$  taken into account. While the shape of the resonance does not much depend on the given value of  $J^P$ , the dependence on  $W$  is different. In particular, the result with  $J^P = 5/2^-$  increases faster than the other ones as  $W$  increases. We found a similar feature in the case of the Regge approach. However,  $W$  increases further, all the results for the total cross sections are lessened as  $W$  increases. Thus, the Regge approach produces the results more consistently than those from the effective Lagrangian method. Secondly, we examined the results for the differential cross sections as functions of the scattering angle with several different values of the CM total energy. The

results in the resonance region clearly are distinguished, as different sets of the spin-parity quantum numbers are used. This implies that the measurement of differential cross sections for the  $K^- p \rightarrow J/\psi \Lambda$  reaction may give a clue on the spin-parity quantum number of  $P_{cs}$ . We also studied the differential cross sections  $d\sigma/dt$  as functions of the CM total energy squared, i.e.,  $s$ . When the scattering angle near  $\theta = 90^\circ$ ,  $s$  dependences of the differential cross sections prominently reveal the differences among the results with different sets of  $J^P$ .

The present results may be used as a theoretical guide for possible future experiments for findings of the hidden-charm pentaquarks with strangeness. Similar studies for other  $P_{cs}$  are also under way.

## ACKNOWLEDGMENTS

The present work was supported by Basic Science Research Program through the National Research Foundation of Korea funded by the Ministry of Education, Science and Technology (Grant No. 2018R1A5A1025563).

- 
- [1] R. Aaij *et al.* (LHCb Collaboration), [arXiv:2012.10380](#).
  - [2] R. Aaij *et al.* (LHCb Collaboration), *Phys. Rev. Lett.* **115**, 072001 (2015).
  - [3] R. Aaij *et al.* (LHCb Collaboration), *Phys. Rev. Lett.* **117**, 082002 (2016).
  - [4] R. Aaij *et al.* (LHCb Collaboration), *Phys. Rev. Lett.* **122**, 222001 (2019).
  - [5] S. K. Choi *et al.* (Belle Collaboration), *Phys. Rev. Lett.* **91**, 262001 (2003).
  - [6] B. Aubert *et al.* (BABAR Collaboration), *Phys. Rev. Lett.* **90**, 242001 (2003).
  - [7] H. X. Chen, W. Chen, X. Liu, and S. L. Zhu, *Phys. Rep.* **639**, 1 (2016).
  - [8] A. Esposito, A. Pilloni, and A. D. Polosa, *Phys. Rep.* **668**, 1 (2017).
  - [9] Y. Dong, A. Faessler, and V. E. Lyubovitskij, *Prog. Part. Nucl. Phys.* **94**, 282 (2017).
  - [10] S. L. Olsen, T. Skwarnicki, and D. Zieminska, *Rev. Mod. Phys.* **90**, 015003 (2018).
  - [11] F. K. Guo, C. Hanhart, U. G. Meißner, Q. Wang, Q. Zhao, and B. S. Zou, *Rev. Mod. Phys.* **90**, 015004 (2018).
  - [12] L. Maiani, A. D. Polosa, and V. Riquer, *Phys. Lett. B* **749**, 289 (2015).
  - [13] G. N. Li, X. G. He, and M. He, *J. High Energy Phys.* **12** (2015) 128.
  - [14] R. Ghosh, A. Bhattacharya, and B. Chakrabarti, *Phys. Part. Nucl. Lett.* **14**, 550 (2017).
  - [15] H. Y. Cheng and C. K. Chua, *Phys. Rev. D* **92**, 096009 (2015).
  - [16] V. V. Anisovich, M. A. Matveev, J. Nyiri, A. V. Sarantsev, and A. N. Semenova, *Int. J. Mod. Phys. A* **30**, 1550190 (2015).
  - [17] Z. G. Wang, *Eur. Phys. J. C* **76**, 142 (2016).
  - [18] H. X. Chen, L. S. Geng, W. H. Liang, E. Oset, E. Wang, and J. J. Xie, *Phys. Rev. C* **93**, 065203 (2016).
  - [19] A. Feijoo, V. K. Magas, A. Ramos, and E. Oset, *Eur. Phys. J. C* **76**, 446 (2016).
  - [20] J. X. Lu, E. Wang, J. J. Xie, L. S. Geng, and E. Oset, *Phys. Rev. D* **93**, 094009 (2016).
  - [21] R. Chen, J. He, and X. Liu, *Chin. Phys. C* **41**, 103105 (2017).
  - [22] C. W. Xiao, J. Nieves, and E. Oset, *Phys. Lett. B* **799**, 135051 (2019).
  - [23] B. Wang, L. Meng, and S. L. Zhu, *Phys. Rev. D* **101**, 034018 (2020).
  - [24] H. X. Chen, W. Chen, X. Liu, and X. H. Liu, *Eur. Phys. J. C* **81**, 409 (2021).
  - [25] F. Z. Peng, M. J. Yan, M. Sánchez Sánchez, and M. P. Valderrama, [arXiv:2011.01915](#).
  - [26] R. Chen, *Eur. Phys. J. C* **81**, 122 (2021).
  - [27] J. J. Wu, R. Molina, E. Oset, and B. S. Zou, *Phys. Rev. Lett.* **105**, 232001 (2010).
  - [28] J. J. Wu, R. Molina, E. Oset, and B. S. Zou, *Phys. Rev. C* **84**, 015202 (2011).
  - [29] S. G. Yuan, K. W. Wei, J. He, H. S. Xu, and B. S. Zou, *Eur. Phys. J. A* **48**, 61 (2012).
  - [30] E. Santopinto and A. Giachino, *Phys. Rev. D* **96**, 014014 (2017).
  - [31] S. Takeuchi and M. Takizawa, *Phys. Lett. B* **764**, 254 (2017).
  - [32] Y. Yamaguchi and E. Santopinto, *Phys. Rev. D* **96**, 014018 (2017).
  - [33] Y. Yamaguchi, A. Giachino, A. Hosaka, E. Santopinto, S. Takeuchi, and M. Takizawa, *Phys. Rev. D* **96**, 114031 (2017).

- [34] Y. Yamaguchi, H. García-Tecocoatzi, A. Giachino, A. Hosaka, E. Santopinto, S. Takeuchi, and M. Takizawa, *Phys. Rev. D* **101**, 091502 (2020).
- [35] J. He, *Eur. Phys. J. C* **79**, 393 (2019).
- [36] Z. G. Wang, *Int. J. Mod. Phys. A* **36**, 2150071 (2021).
- [37] J. Ferretti, E. Santopinto, M. Naeem Anwar, and M. A. Bedolla, *Phys. Lett. B* **789**, 562 (2019).
- [38] J. Ferretti and E. Santopinto, *J. High Energy Phys.* 04 (2020) 119.
- [39] M. I. Eides, V. Y. Petrov, and M. V. Polyakov, *Mod. Phys. Lett. A* **35**, 2050151 (2020).
- [40] H. Noumi, *Proc. Sci., Hadron2013* (2013) 031.
- [41] K. Shirotori *et al.*, *J. Phys. Conf. Ser.* **569**, 012085 (2014).
- [42] S. H. Kim, A. Hosaka, H.-Ch. Kim, H. Noumi, and K. Shirotori, *Prog. Theor. Exp. Phys.* **2014**, 103D01 (2014).
- [43] S. H. Kim, A. Hosaka, H.-Ch. Kim, and H. Noumi, *Phys. Rev. D* **92**, 094021 (2015).
- [44] S. H. Kim, H.-Ch. Kim, and A. Hosaka, *Phys. Rev. D* **94**, 094025 (2016).
- [45] Q. F. Lü, X. Y. Wang, J. J. Xie, X. R. Chen, and Y. B. Dong, *Phys. Rev. D* **93**, 034009 (2016).
- [46] S. H. Kim, H.-Ch. Kim, and A. Hosaka, *Phys. Lett. B* **763**, 358 (2016).
- [47] J. Kodaira and K. Sasaki, *Lett. Nuovo Cimento* **26**, 417 (1979).
- [48] M. Guidal, J. M. Laget, and M. Vanderhaeghen, *Nucl. Phys. A* **627**, 645 (1997).
- [49] T. Mart, S. Clymton, and A. J. Arifi, *Phys. Rev. D* **92**, 094019 (2015).
- [50] S. H. Kim, S. i. Nam, Y. Oh, and H.-Ch. Kim, *Phys. Rev. D* **84**, 114023 (2011).
- [51] Q. Wang, X. H. Liu, and Q. Zhao, *Phys. Rev. D* **92**, 034022 (2015).
- [52] E. Y. Paryev and Y. T. Kiselev, *Nucl. Phys.* **A978**, 201 (2018).
- [53] X. Y. Wang, J. He, X. R. Chen, Q. Wang, and X. Zhu, *Phys. Lett. B* **797**, 134862 (2019).
- [54] K. Jenkins *et al.* *Phys. Rev. D* **17**, 52 (1978).
- [55] I. H. Chiang *et al.* *Phys. Rev. D* **34**, 1619 (1986).
- [56] P. A. Zyla *et al.* (Particle Data Group), *Prog. Theor. Exp. Phys.* **2020**, 083C01 (2020).
- [57] W. Rarita and J. Schwinger, *Phys. Rev.* **60**, 61 (1941).
- [58] A. Ali *et al.* (GlueX Collaboration), *Phys. Rev. Lett.* **123**, 072001 (2019).
- [59] C. W. Xiao, J. J. Wu, and B. S. Zou, *Phys. Rev. D* **103**, 054016 (2021).
- [60] S. H. Kim, S. i. Nam, A. Hosaka, and H.-Ch. Kim, *Phys. Rev. D* **88**, 054012 (2013).
- [61] T. A. Rijken, M. M. Nagels, and Y. Yamamoto, *Prog. Theor. Phys. Suppl.* **185**, 14 (2010).
- [62] T. Barnes and X. Li, *Phys. Rev. D* **75**, 054018 (2007).
- [63] J. Y. Kim and H.-Ch. Kim, *Phys. Rev. D* **97**, 114009 (2018).
- [64] A. Donnachie, H. G. Dosch, P. V. Landshoff, and O. Nachtmann, *Pomeron Physics and QCD* (Cambridge University Press, Cambridge, England, 2002).
- [65] S. H. Kim, S. i. Nam, D. Jido, and H.-Ch. Kim, *Phys. Rev. D* **96**, 014003 (2017).
- [66] A. I. Titov and B. Kampfer, *Phys. Rev. C* **78**, 025201 (2008).
- [67] S. H. Kim, Y. Oh, and A. I. Titov, *Phys. Rev. C* **95**, 055206 (2017).
- [68] M. M. Brisudova, L. Burakovsky, and J. T. Goldman, *Phys. Rev. D* **61**, 054013 (2000).
- [69] T. Corthals, J. Ryckebusch, and T. Van Cauteren, *Phys. Rev. C* **73**, 045207 (2006).
- [70] J. K. Storrow, *Phys. Rep.* **103**, 317 (1984).